BJA

British Journal of Anaesthesia, 122 (5): 613–621 (2019)

doi: 10.1016/j.bja.2019.02.010
Advance Access Publication Date: 20 March 2019
Clinical Practice

Permeabilised skeletal muscle reveals mitochondrial deficiency in malignant hyperthermia-susceptible individuals

Leon Chang[1], Catherine Daly[2], Dorota M. Miller[1], Paul D. Allen[1], John P. Boyle[3], Philip M. Hopkins[1,2,*] and Marie-Anne Shaw[1]

[1]Leeds Institute of Medical Research at St. James's, University of Leeds, Leeds, UK, [2]Malignant Hyperthermia Unit, St James's University Hospital, Leeds, UK and [3]Leeds Institute of Cardiovascular and Metabolic Medicine, University of Leeds, Leeds, UK

*Corresponding author. E-mail: p.m.hopkins@leeds.ac.uk

Abstract

Background: Individuals genetically susceptible to malignant hyperthermia (MH) exhibit hypermetabolic reactions when exposed to volatile anaesthetics. Mitochondrial dysfunction has previously been associated with the MH-susceptible (MHS) phenotype in animal models, but evidence of this in human MH is limited.
Methods: We used high resolution respirometry to compare oxygen consumption rates (oxygen flux) between permeabilised human MHS and MH-negative (MHN) skeletal muscle fibres with or without prior exposure to halothane. A substrate-uncoupler-inhibitor titration protocol was used to measure the following components of the electron transport chain under conditions of oxidative phosphorylation (OXPHOS) or after uncoupling the electron transport system (ETS): complex I (CI), complex II (CII), CI+CII and, as a measure of mitochondrial mass, complex IV (CIV).
Results: Baseline comparisons without halothane exposure showed significantly increased mitochondrial mass (CIV, $P=0.021$) but lower flux control ratios in $CI+CII_{(OXPHOS)}$ and $CII_{(ETS)}$ of MHS mitochondria compared with MHN ($P=0.033$ and 0.005, respectively) showing that human MHS mitochondria have a functional deficiency. Exposure to halothane triggered a hypermetabolic response in MHS mitochondria, significantly increasing mass-specific oxygen flux in $CI_{(OXPHOS)}$, $CI+CII_{(OXPHOS)}$, $CI+CII_{(ETS)}$, and $CII_{(ETS)}$ ($P=0.001–0.012$), while the rates in MHN samples were unaltered by halothane exposure.
Conclusions: We present evidence of mitochondrial dysfunction in human MHS skeletal muscle both at baseline and after halothane exposure.

Keywords: electron transport chain; malignant hyperthermia; mitochondria, oxidative phosphorylation; skeletal muscle; volatile anaesthetic

Editorial decision: 04 February 2019; **Accepted:** 4 February 2019

Editor's key points

- The effect of malignant hyperthermia susceptibility (MHS) on skeletal muscle mitochondrial function in humans is uncertain.
- We compared oxygen consumption using high resolution respirometry in MHS and normal human skeletal muscle fibres.
- Muscle from MHS individuals had increased mitochondrial mass but reduced oxidative capacity compared with normal individuals.
- Impaired mitochondrial function in human MHS skeletal muscle may result from chronic elevation of myoplasmic Ca^{2+}.

Malignant hyperthermia (MH) is a hypermetabolic reaction triggered by potent inhalation anaesthetics in susceptible individuals.[1] Direct consequences of the hypermetabolic state are increased carbon dioxide production, increased oxygen consumption, metabolic acidosis, and hyperthermia, with reflex sympathetic stimulation.[2] Ultimately, skeletal muscle adenosine triphosphate (ATP) production fails to keep up with energy requirements leading to muscle rigidity and rhabdomyolysis.[2] Variants in the *RYR1* gene that encodes the skeletal muscle Ca^{2+} release channel (ryanodine receptor, RyR1)[3] or the *CACNA1S* gene that encodes the sarcolemmal slow voltage-gated Ca^{2+} channel that acts as the voltage sensor for excitation-contraction (EC) coupling (dihydropyridine receptor)[4,5] are associated with MH in 76% of UK MH families.[6] Both proteins work in concert to regulate Ca^{2+} concentrations in skeletal muscle at rest and during EC coupling.[7]

Before the discovery of genetic linkage between *RYR1* and MH susceptibility,[8,9] several researchers postulated an important role for mitochondria in the development of an MH reaction. Recent findings in transgenic mice with *RYR1* mutation knock-in has rekindled interest in such a role for mitochondria.[10–12] There is also the implication that mitochondrial dysfunction may explain why some MH-susceptible (MHS) individuals experience myopathic traits such as muscle weakness and exercise intolerance.[13]

Some of the earliest observations in MH mitochondria were conducted on the MH porcine model, which showed halothane-induced inhibition of complex I (CI).[14,15] Research on *RYR1* mutation knock-in mouse models has found mitochondrial abnormalities with various degrees of severity depending on the *RyR1* mutation. Notable observations include lower oxidative phosphorylation (OXPHOS), increased oxidative stress, and increased reactive oxygen species (ROS) production.[10–12] Structural mitochondrial deformity, an indication of damage, including a loss of cristae organisation and mitochondrial swelling, has been observed in multiple reports using electron microscopy. This suggests there may be metabolic dysfunction and altered OXPHOS in muscles from both MHS mice[10,16] and humans.[17,18]

In contrast to animal models, research on human MH mitochondrial function is lacking. Despite the structural abnormalities seen in MHS humans,[17,18] evidence for functional defects is conflicting. Some reports suggest normal OXPHOS and respiratory control in mitochondria of MHS humans,[19] whilst others have claimed impaired OXPHOS and ATP production after bouts of training in MHS individuals.[20] The discrepancies may be explained by variation in sample type, methodology, or both. We investigated whether mitochondrial dysfunction is present in *ex vivo* skeletal muscle from MHS humans under basal conditions and after exposure to the MH trigger agent halothane.

Methods

Patients

Patients considered for inclusion in this study were those attending for investigation of their susceptibility to MH. The reason for investigation was a clinical suspicion of increased risk either because of an adverse reaction to anaesthesia consistent with MH, or because a family member was known to be MHS. The majority of index case patients had been found not to harbour a pathogenic variant (www.emhg.org) in *RYR1* and *CACNA1S* before attending for further investigation, which involved an open muscle biopsy and subsequent *in vitro* contracture testing (IVCT). Family members were either from families where no pathogenic variant had been found or who had been found not to carry a familial variant. Patients gave written informed consent to the study that was approved by Leeds (East) Research Ethics Committee (Leeds, UK, reference 10/H1306/70).

Patients were diagnosed using the IVCT as either MHS or MH negative (MHN) according to the protocol of the European MH Group.[21] The laboratory classification of MHS is subdivided into MHS_{hc} (samples respond abnormally to both halothane and caffeine challenges), MHS_h (samples respond abnormally to halothane but normally to caffeine challenge), or MHS_c (samples respond abnormally to caffeine but normally to halothane challenge).

Muscle samples

Diagnostic muscle biopsies and IVCT were conducted according to the protocol of the European MH Group,[21] and prepared by a protocol adapted from that described.[22,23] In brief, six muscle fascicles (typical dimensions 25×4×3 mm) were excised from the *vastus medialis* under femoral nerve block and immediately placed in oxygenated Krebs' solution (NaCl 118.1 mM, KCl 3.4 mM, $MgSO_4$ 0.8 mM, KH_2PO_4 1.2 mM, glucose 11.1 mM, $NaHCO_3$ 25.0 mM, $CaCl_2$ 2.5 mM, pH 7.4) at room temperature and taken to the MH laboratory. There, samples were kept at room temperature in Krebs solution, which was gassed continuously with carbogen (O_2 95%, CO_2 5%) until IVCT. This study required both a muscle fascicle that had not been used for the diagnostic challenge tests (baseline) and a fascicle that had been used in the static halothane test (halothane-exposed). At the end of the halothane test, the halothane-exposed and baseline samples were each placed into 1 ml of ice-cold biopsy preservation buffer, BIOPS (CaK_2EGTA 2.77 mM, K_2EGTA 7.23 mM, Na_2ATP 5.77 mM, $MgCl_2 \cdot 6H_2O$ 6.56 mM, taurine 20 mM, Na_2phosphocreatine 15 mM, imidazole 20 mM, dithiothreitol 0.5 mM, and MES hydrate 50 mM, pH 7.1, adjusted with KOH 5 N at 0°C). Samples were then placed in a Petri dish with ice-cold BIOPS and separated using sharp forceps to obtain small muscle fibre bundles containing ~4–5 fibres each. These samples then underwent chemical permeabilisation in BIOPS containing saponin (50 μg ml^{-1}) for 30 min, before being washed with 1 ml respiration medium, Mir05 (EGTA 0.5 mM, $MgCl_2 \cdot 6H_2O$ 3 mM, lactobionic acid 60 mM, taurine 20 mM, KH_2PO_4 10 mM, 4-(2-hydroxyethyl)-1-piperazineethanesulfonic acid 20 mM adjusted to pH 7.1 with KOH at 37°C, D-sucrose 110 mM, and 1 g L^{-1} essentially fatty acid free bovine serum albumin) to remove residual saponin. The sample was then taken and blot-dried for 5 s, before being

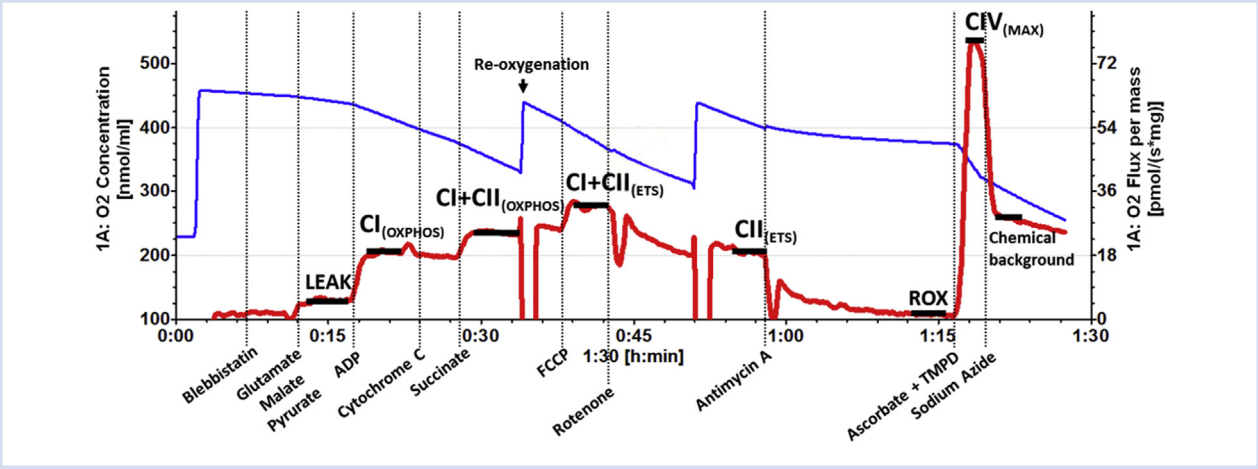

Fig. 1. Example high resolution respirometry trace showing the rate of oxygen flux (red line) over time after sequential titration of substrates and inhibitors, expressed as pmol s^{-1} mg^{-1}. The blue line represents oxygen concentrations within the chamber (nmol ml^{-1}). Vertical dashed lines represent timepoints where substrates have been added. The horizontal black lines which overlay the red line plateaus indicate the position of datapoints. ADP, adenosine diphosphate; CI, complex I; CII, complex II; CIV, complex IV; ETS, electron transport system; FCCP, carbonyl cyanide 4-(trifluoromethoxy)-phenylhydrazone; OXPHOS, oxidative phosphorylation; ROX, residual oxygen flux; TMPD, N,N,N′,N'-tetramethyl-p-phenylenediamine.

weighed and loaded into the respirometer chambers (5–10 mg in each chamber) containing Mir05 2 ml. The time between biopsy collection and assay time was ~90–120 min.

High resolution respirometry

Oxygen consumption over time was measured using Oroboros respiratory analysers (Oroboros Instruments, Innsbruk, Austria) at 2 s intervals with polarographic oxygen sensors, and expressed as mass-specific oxygen flux (pmol s^{-1} mg^{-1}). The analyser was calibrated daily in air saturated solution before experimentation. Assays were initiated by injecting oxygen into each chamber to raise the oxygen concentration to >400 nmol ml^{-1} before a substrate-uncoupler-inhibitor titration (SUIT) protocol. Re-oxygenation of the chambers was performed to maintain oxygen concentration at 200–500 nmol ml^{-1} to prevent limitation because of oxygen diffusion.[23] Each assay was performed at 37°C, with chamber stirrers set at 750 rpm.

SUIT protocol

An adapted SUIT protocol was used to investigate the OXPHOS capacity of individual complexes and respiratory states[22,23] (Fig 1). The procedure was initiated with addition of blebbistatin 5 μM to prevent spontaneous contraction of muscle fibres.[24] Glutamate (10 mM), malate (0.5 mM), and pyruvate (5 mM) were then added to facilitate measurements of CI respiration in the absence of adenosine diphosphate (ADP) (LEAK respiration- electron flow coupled to proton pumping to compensate for proton leaks). ADP (2.5 mM) is then added to allow measurement of maximal CI-supported OXPHOS ($CI_{[OXPHOS]}$). At this point, outer mitochondrial membrane integrity was assessed by the addition of cytochrome c 10 μM. Samples with increased respiration rates of >10% after addition of cytochrome c, which indicates outer mitochondrial membrane damage, were excluded from analysis.

Once membrane integrity had been assessed, maximal activity of complex II (CII) was stimulated with addition of succinate (10 mM). Oxygen flux at this stage ($CI+CII_{[OXPHOS]}$) reflects the combined activities of CI and CII, and is regarded as the maximum OXPHOS capacity in the coupled state. Next, stepwise additions of carbonyl cyanide 4-(trifluoromethoxy)-phenylhydrazone (FCCP) (0.5 μM) were made until there was no further increase in oxygen flux. FCCP uncouples the electron transport system (ETS) by collapsing the proton gradient between the intermembrane space and the mitochondrial matrix providing the maximum ETS capacity ($CI+CII_{[ETS]}$). After uncoupling the system, electron flow through CI was inhibited using rotenone (0.5 μM), providing maximum CII activity alone ($CII_{[ETS]}$). Finally, antimycin A was introduced to inhibit complex III (CIII). CIII activity contributes to all datapoints aside from the complex IV (CIV) assay. However, its activity is not measured directly in this protocol as it obtains electrons downstream of CI and CII. Residual oxygen flux present after addition of antimycin A is a result of non-mitochondrial respiration that is subtracted from each respiratory state reading before analysis.

Complex IV assay

Measurement of mass-specific CIV oxygen flux was used as an alternative proxy marker for estimations of mitochondrial content. Ascorbate (2 mM) and N,N,N′,N'-tetramethyl-p-phenylenediamine (0.5 mM) were applied at the end of the standard SUIT protocol. Measurement of CIV flux was taken at the peak of the corresponding trace, and residual chemical background was removed from this value by applying sodium azide (10 mM).[25]

Data handling and analysis

Raw data in the form of oxygen flux per muscle mass (pmol s^{-1} mg^{-1}) includes the confounding effects of both mitochondrial quality and quantity. Data from samples with and without halothane exposure were internally normalised to the common reference state, $CI+CII_{(ETS)}$ (maximum uncoupled respiration). Normalised oxygen flux per mass is presented as flux control ratios (FCR) which highlight differences in mitochondrial function, as a proportion of the reference state, which is independent of mitochondrial content.

Table 1 Summary of characteristics of the patients contributing samples for this study. The *RYR1* variants are annotated for their likely pathogenicity using the criteria of Miller and colleagues[6] as: *unlikely pathogenic; †potentially pathogenic; ‡likely pathogenic; and ¶pathogenic. *In vitro* contracture testing (IVCT) data for each MHS individual is available in Supplementary Table S1. MHN, malignant hyperthermia-negative; MHS, malignant hyperthermia-susceptible; MHS_h, abnormal response in the *in vitro* contracture test to halothane but not caffeine; MHS_{hc}, abnormal response in the *in vitro* contracture test to halothane and caffeine

	MHN (n=36)	MHS (n=23)					
		MHS_h (n=12)			MHS_{hc} (n=11)		
Male:female	16:20	5:7			7:4		
Age at biopsy (yr)	(11–68)	(12–64)			(12–57)		
Individuals with at least one *RYR1* variant	–	8			10		
RYR1 variants found	–	**Nucleotide change**	**Amino acid change**	**Accession number**	**Nucleotide change**	**Amino acid change**	**Accession number**
		c.251C>T†	p.Thr84Met	rs186983396	c.455C>A†	p.Ala152Asp	–
		c.4178A>G*	p.Lys1393Arg	rs137933390	c.1202G>A‡	p.Arg401His	rs193922766
		c.5183C>T‡	p.Ser1728Phe	rs193922781	c.8729C>T†	p.Tyr2910Met	–
		c.6670C>T†	p.Arg2224Cys	rs199870223	c.10357C>T†	p.Arg3453Cys	rs1482429489
		c.6785G>A†	p.Gly2262Asp	–	c.11132C>T‡	p.Thr3711Met	rs375915752
		c.7879G>A‡	p.Val2627Met	–	c.11958C>G‡	p.Asp3986Glu	rs193922842
		c.12860C>T†	p.Ala4287Val	–	c.12700G>C‡	p.Val4234Leu	rs193922852
		c.14210G>A[c]	p.Arg4737Gln	rs193922868	c.7879G>A‡	p.Val2627Met	–
		c.4293G>A	p.Thr1431=	rs727504130	c.1021G>A¶	p.Gly341Arg	rs121918592

Oxygen flux recorded from each sample trace was exported from proprietary software (DatLab5, Oroboros Instruments) into Microsoft Excel (Microsoft Inc, Redmond, Washington, USA) before analysis using IBM (Armonk, NY, USA) SPSS statistics version 21. Pairwise comparisons were performed using a combination of Wilcoxon signed-rank tests to assess the effects of halothane exposure and Mann–Whitney *U*-tests to assess median differences between baseline controls. Further analysis of MHS subgroups used the Kruskal–Wallis test and *post hoc* Dunn's procedure to identify differences between patients classified as MHN, MHS_h, and MHS_{hc}. Data were summarised as boxplots using

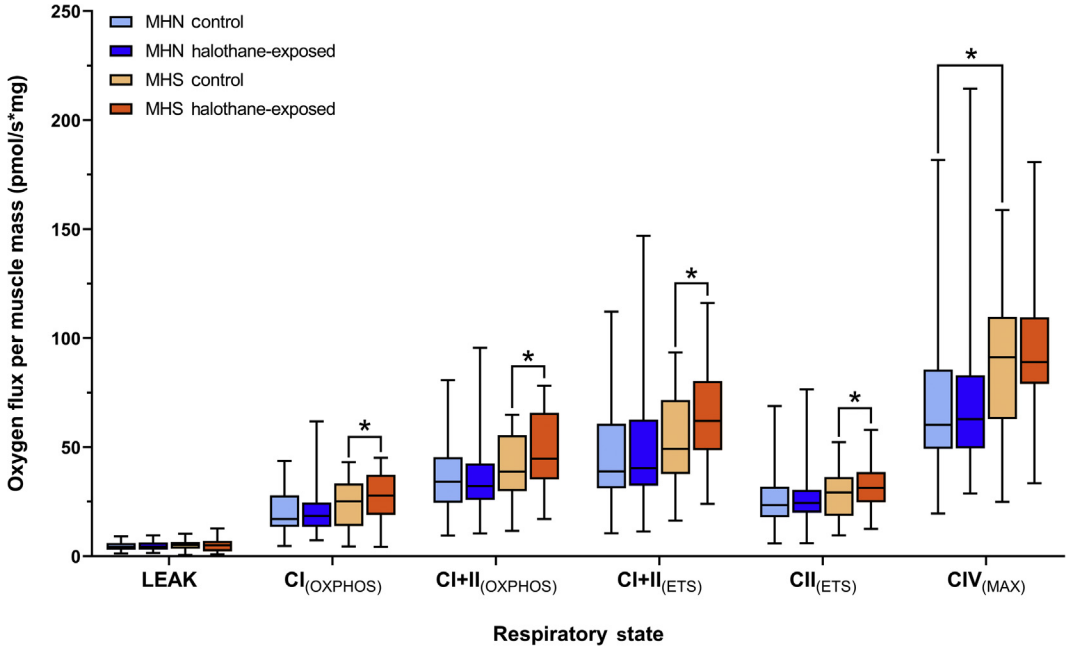

Fig. 2. High resolution respirometry of permeabilised *vastus medialis* biopsies from MHN (n= 36) and MHS (n=23) individuals. Boxplots show median, inter-quartile range (IQR) and min-max range for each phenotype in control and halothane-exposed samples. Statistically significant pairwise comparisons (P<0.05) are labelled with an asterisk (refer to Table 2 for exact P-values). CI, complex I; CII, complex II; CIV, complex IV; ETS, electron transport system; MHN, malignant hyperthermia-negative; MHS, malignant hyperthermia-susceptible; OXPHOS, oxidative phosphorylation.

Table 2 Summary of statistical comparisons for each data set, outlining *P*-values for each pairwise comparison between and within phenotype for the mass-specific oxygen flux (pmol s^{-1} mg^{-1}) and flux control ratio (FCR) readings. The *P*-values for FCR differences between MHS subgroups are also included with *post hoc* statistics for each comparison. *P*-values reaching statistical significance are presented in bold font. ETS, electron transport system; MHN, malignant hyperthermia-negative; MHS, malignant hyperthermia-susceptible; MHS_h, abnormal response in the *in vitro* contracture test to halothane but not caffeine; MHS_{hc}, abnormal response in the *in vitro* contracture test to halothane and caffeine; OXPHOS, oxidative phosphorylation

Respiratory state	Oxygen consumption rate (pmol s^{-1} mg^{-1})		
	MHN	MHS	MHN *vs* MHS
	Control *vs* halothane-exposure (*P*-value)		Control comparisons (*P*-value)
Leak	0.944	0.429	0.732
$CI_{(OXPHOS)}$	0.593	**0.012**	0.113
$CI+CII_{(OXPHOS)}$	0.789	**0.005**	0.071
$CI+CII_{(ETS)}$	0.157	**0.003**	0.050
$CII_{(ETS)}$	0.057	**0.001**	0.376
$CIV_{(MAX)}$	0.718	0.101	**0.021**
Respiratory state	Flux control ratio (FCR)		
	MHN	MHS	MHN vs MHS
	Control *vs* halothane-exposure (*P*-value)		Control comparisons (*P*-value)
LEAK	0.753	0.362	0.074
$CI_{(OXPHOS)}$	0.480	**0.007**	0.534
$CI+CII_{(OXPHOS)}$	0.470	**0.003**	**0.033**
$CI+CII_{(ETS)}$			
$CII_{(ETS)}$	**0.041**	**0.001**	**0.005**
$CIV_{(MAX)}$	0.307	0.052	0.913

Respiratory state	FCR differences (halothane-exposed - control)			
	Kruskal-Wallis (*P*-value)	*Post hoc* (*P*-value)		
		MHN *vs* MHS_h	MHN *vs* MHS_{hc}	MHS_h *vs* MHS_{hc}
LEAK	0.349			
$CI_{(OXPHOS)}$	0.209			
$CI+CII_{(OXPHOS)}$	**0.043**	1.000	**0.036**	0.390
$CI+CII_{(ETS)}$	0.086			
$CII_{(ETS)}$	0.263			
$CIV_{(MAX)}$	0.532			

GraphPad Prism 8 (GraphPad Software Inc, San Diego, CA, USA). There are no published data on the magnitude of changes in OXPHOS variables that are associated with human pathology. Preliminary data from a transgenic mouse model of MH suggested that there was a standardised mean difference of 0.86 in baseline $CI+CII_{(ETS)}$ between MHS and MHN mice. Such a difference would be detected with a sample size of 12 in each group with $\alpha<0.05$ and $\beta<0.2$. We sought to identify changes with a standardised difference in means of >0.75, as this is generally accepted as a relevant effect size in biological systems. On the basis that more people tested by the MH Unit prove to be MHN rather than MHS, we planned to include samples from 23 MHS and at least 35 MHN, in order to achieve $\alpha<0.05$ and $\beta<0.2$. These numbers of samples enable detection of paired (with and without halothane exposure) standardised mean differences of 0.6 and 0.5 for MHS and MHN samples, respectively.

Results

Patient characteristics

A summary of patient characteristics is presented in Table 1. Eighteen of the 23 MHS group were subsequently found to carry at least one variant in the *RYR1* gene and these variants are also listed in Table 1. None of the patients had clinical or histopathological features suggestive of a mitochondrial myopathy. We included 59 individuals from 52 families: the maximum number from any family was two individuals.

Mass-specific oxygen flux comparisons

Oxygen flux per milligram of muscle was compared between MHN and MHS samples, with or without exposure to halothane (Fig 2). Comparisons of samples without halothane exposure showed no differences between the two phenotypes aside from $CIV_{(MAX)}$, where MHS samples had a significantly greater oxygen flux compared with MHN ($P=0.021$), suggesting higher mitochondrial content in MHS samples. Pairwise comparisons showed that oxygen flux was significantly elevated in MHS samples after halothane exposure for $CI_{(OXPHOS)}$, $CI+CII_{(OXPHOS)}$, $CI+CII_{(ETS)}$, and $CII_{(ETS)}$ (Table 2). The rates in MHN samples were unaltered by halothane exposure.

Flux control ratio (normalised oxygen flux)

Mass-specific oxygen flux was normalised to a common reference state (control $CI+CII_{(ETS)}$) to generate FCR to remove the confounding effects of mitochondrial content differences between samples (Fig 3). Comparisons of FCR at baseline

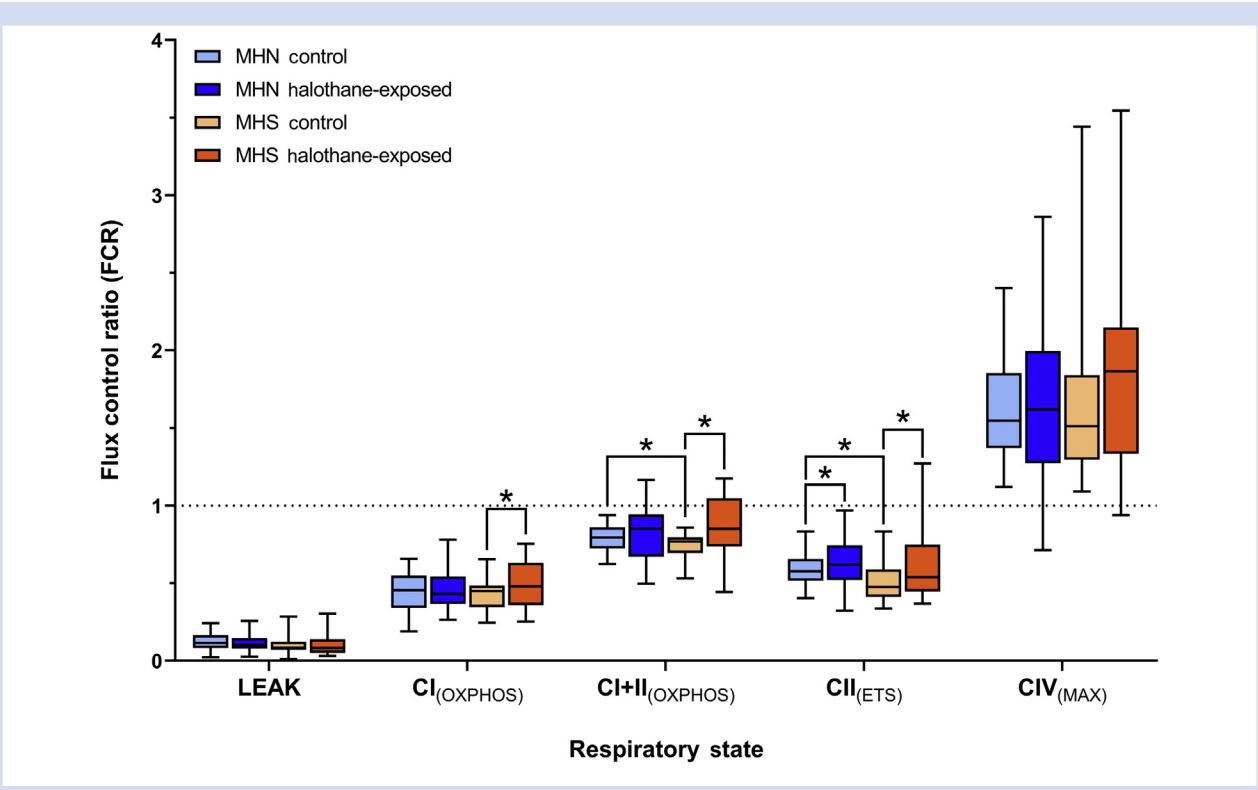

Fig. 3. Boxplot comparison of flux control ratios (FCR) from MHN (n=36) and MHS (n=23) control and halothane-exposed samples. FCR are generated by internally normalising oxygen flux per muscle mass to the non-halothane-exposed control CI+CII$_{(ETS)}$ (indicated by the horizontal dashed line). Boxplots show median, inter-quartile range (IQR) and min-max range for each phenotype in control and halothane-exposed samples. Statistically significant pairwise comparisons (P<0.05) are labelled with an asterisk (refer to Table 2 for exact P-values). CI, complex I; CII, complex II; CIV, complex IV; ETS, electron transport system; MHN, malignant hyperthermia-negative; MHS, malignant hyperthermia-susceptible; OXPHOS, oxidative phosphorylation.

revealed that CI+CII$_{(OXPHOS)}$ and CII$_{(ETS)}$ were significantly lower in MHS samples compared with MHN (P=0.033 and 0.005, respectively, Table 2), suggesting functional deficiency. Normalised CIV$_{(MAX)}$ showed no significant differences between MHS and MHN controls, indicating similar functional capacity of CIV. FCR comparisons between control and halothane-exposed samples support the findings seen in the mass-specific dataset, with statistically significant findings in several of the same respiratory states (Table 2). However, one exception was found in MHN CII$_{(ETS)}$ which increased after halothane-exposure (P=0.041).

Flux control ratio responses within the subdivided MHS phenotypes

FCR were used for further analysis within the MHS phenotype, comparing the magnitude of change with and without exposure to halothane between the MHS$_h$ and MHS$_{hc}$ phenotypes (Fig 4); there were no patients in this sample categorised as MHS$_c$. Results from the Kruskal–Wallis test showed that CI+CII$_{(OXPHOS)}$ responses differed significantly between MH phenotypes after halothane exposure (Table 2). *Post hoc* analysis showed that these differences in response between MHN and MHS groups were largely attributable to responses of the MHS$_{hc}$ subgroup, as there were no significant differences in response to halothane exposure between the MHN group and the MHS$_h$ subgroup.

Discussion

Baseline comparisons using mass-specific flux showed higher CIV$_{(MAX)}$ in MHS compared with MHN muscle, which indicates a greater mass of mitochondria in MHS muscle per milligram of tissue. Alternative mitochondrial markers such as citrate synthase and mtDNA were considered for this study, but the CIV assay was chosen as it can be performed during the experiment and allows measurements on the same exact sample, avoiding issues with degradation. To normalise for differences in mitochondrial mass, we compared FCR data which showed that there were functional deficits in MHS muscle as well. The CI+CII$_{(OXPHOS)}$ and CII$_{(ETS)}$ FCR were significantly lower in MHS samples compared with MHN, which implies that there is uncoupling of mitochondria in MHS muscle in addition to CII deficiency, both of which would likely result in inefficient ATP production. The uncoupling of MHS mitochondria is perhaps a side-effect of the swelling and structural abnormalities seen in previous human studies,[18] or a consequence of chronically elevated myoplasmic Ca^{2+}concentration in MHS muscle (see below). As no significant differences in CI$_{(OXPHOS)}$ were found, CII deficiency seems to be the primary cause for the reduced maximum OXPHOS capacity of MHS muscle as defined by CI+CII$_{(OXPHOS)}$ FCR. This is of great importance, as a lower OXPHOS capacity suggests that the ETS in MHS mitochondria is less tightly coupled, and therefore less efficient at producing ATP than in MHN mitochondria. CII, also known as succinate

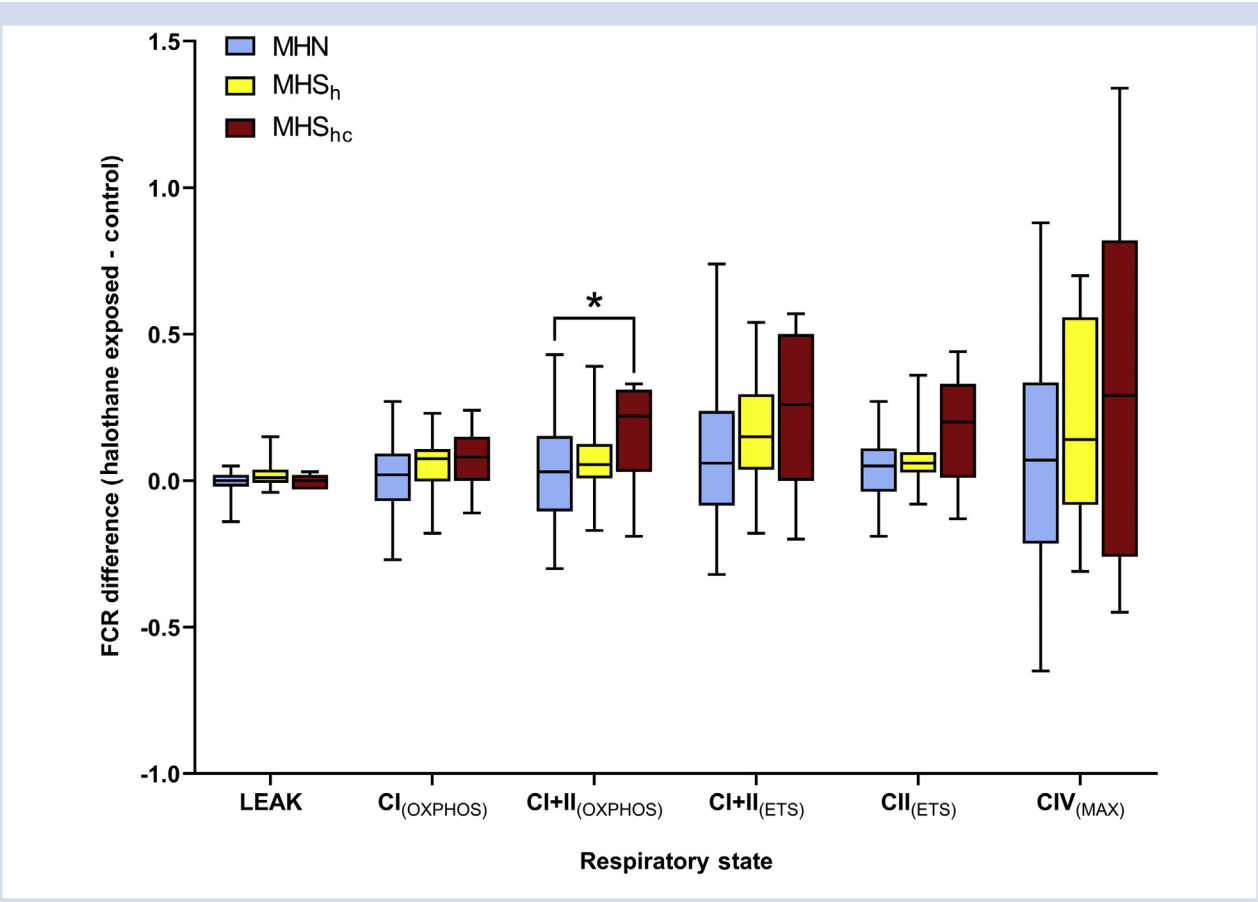

Fig. 4. Boxplot comparison showing the change flux control ratios (FCR) (halothane-exposed control) for each respiratory state. MHN samples (n=36) were plotted with MHS samples (n=23), further split into MHS_h (n=12) and MHS_{hc} (n=11) subgroups. Boxplots show median, inter-quartile range (IQR) and min-max response range for each phenotype. Comparisons labelled with an asterisk show statistically significant *post hoc* pairwise comparisons (refer to Table 2 for exact *P*-values). CI, complex I; CII, complex II; CIV, complex IV; ETS, electron transport system; MHN, malignant hyperthermia-negative; MHS, malignant hyperthermia-susceptible; MHS_h, abnormal response in the *in vitro* contracture test to halothane but not caffeine; MHS_{hc}, abnormal response in the *in vitro* contracture test to halothane and caffeine; OXPHOS, oxidative phosphorylation.

dehydrogenase, is the only component of the ETS that is encoded entirely by nuclear genes and has roles in both OXPHOS and the Krebs cycle, indirectly affecting glycolysis.[26] CII deficiency has not previously been linked to MH susceptibility and its deficiency may mean that the glycolytic function of MHS muscle is also impaired, a potential area for further research. Collectively these findings also suggest a potential compensation mechanism, in which MHS muscle upregulates mitochondrial number to counteract deficiencies in mitochondrial function, hence the similar baseline oxygen flux per unit of muscle mass.

The proposed concept of mitochondrial deficiency in MHS muscle is consistent with that seen in other studies,[11,15,20] but some findings are conflicting. For example, Giulivi and colleagues[11] found a decrease in mitochondrial content, reduced oxygen uptake using malate-glutamate and succinate, and CI, CIII, and CIV deficiency in RyR1 R163C knock-in mice when compared with wild-type. In contrast, we showed evidence of human MHS muscle having higher mitochondrial content, deficiency in succinate-facilitated oxygen flux, with activity deficits in CII only. These discrepancies may be a result of species differences, but they could also be explained by differences in methodology. Giulivi and colleagues[11] used isolated mitochondria in the assessment of mitochondrial content and protein complex function, whereas we used permeabilised muscle fibres. Permeabilised muscle allows interplay between the mitochondria, sarcoplasmic reticulum, and RyR1, which we believe is crucial to accurately assess the biological effects of MH. Furthermore, the oxygen uptake assay in the mouse study was conducted at 22°C, whereas we used 37°C, as the assay temperature significantly impacts OXPHOS capacity.[27]

One hypothesis for the mitochondrial dysfunction in MHS muscle observed here is the result of chronic elevation in cytosolic Ca^{2+}, as has been demonstrated in human[28] and porcine[29] MH muscle, and knock-in mouse models.[11,12,30] Ca^{2+} increases mitochondrial activity which can stimulate higher rates of ROS production through CI, CII, and CIII of the electron transport chain.[31] Increased ROS production has been observed in MH *RYR1* knock-in mice[11] and it is possible that this may translate into human MHS muscle. Increased ROS production, which can cause DNA damage and structural damage to organelles, could explain the mitochondrial swelling seen in previous ultrastructural studies.[10,16,18] Ca^{2+} is also a positive

regulator of the mitochondrial permeability transition pore (MPTP) of the inner mitochondrial membrane.[32] Opening of the MPTP decreases the proton gradient across the inner mitochondrial membrane, which is associated with uncoupling of the electron transport chain from OXPHOS.[33]

Increased activity of several mitochondrial respiratory states is involved in the hypermetabolic response in MHS mitochondria after exposure to halothane. This could simply be a response driven by conversion of myoplasmic adenosine triphosphate (ATP) to ADP, but Díaz-Vegas and colleagues[34] have recently demonstrated a more direct link between skeletal muscle mitochondrial stimulation and activation of RyR1. This may be the result of sarcoplasmic reticulum Ca^{2+} efflux from activated RyR1 in MHS muscle and uptake by mitochondria. Increased intramitochondrial Ca^{2+} stimulates dehydrogenase enzymes, which in turn increases NADH (reduced form of nicotinamide adenine dinucleotide) and ATP production.[35,36] The rhabdomyolysis and cell death that occur in a fulminant MH reaction may partly be caused by the failure of skeletal muscle mitochondria to maintain ATP production to accommodate the Ca^{2+}-stimulated state, along with apoptotic mechanisms activated by increased intramitochondrial Ca^{2+}. The FCR of MHN $CII_{(ETS)}$ also increased after exposure to halothane, suggesting a non-RyR1-mediated component of this effect of halothane. However, the clinical relevance of this phenomenon is uncertain, as it occurs in an artificially uncoupled non-physiological state.

A recent study of Canadian MHS patients found that those who responded abnormally to halothane, but not caffeine, in the caffeine-halothane contracture test, had a higher index of Ca^{2+}-related changes in cultured skeletal muscle cells than patients who responded abnormally to halothane and caffeine.[37] We compared the magnitude of FCR changes in MHS_h and MHS_{hc} fibres and found a significantly greater effect of halothane exposure on $(CI+CII_{[OXPHOS]})$ in MHS_{hc} muscle, which is what we expected, although it is at odds with what might have been anticipated from the work of Figueroa and colleagues.[37] This potential discrepancy might be explained by the use of cultured myotubes by Figueroa and colleagues,[37] whereas we studied adult muscle fibres.

Another unexpected observation was the lack of change in $CI_{(OXPHOS)}$ after halothane treatment. CI activity was reduced by halothane in MH pigs,[11,12] but research in other models has suggested that this effect is independent of the MH trait. Porcine heart mitochondria have shown reversible dose-dependent inhibition of CI (NADH oxidoreductase) after exposure to isoflurane, sevoflurane, or halothane; the latter was the most potent agent.[38] Research using the CI mutant *gas-1 Caenorhabditis elegans* model has also shown evidence of decreased CI function and increased sensitivity to potent inhalation anaesthetics.[39,40] This was not observed in our MHS or MHN muscle and may be because of the inhibitory effects of halothane on CI being both acute and reversible. Such changes would not be detected using our protocol, because of the time delay between halothane exposure and measurement of mitochondrial function (~90–120 min). In addition, previous studies with halothane treatment have used isolated mitochondria taken out of the normal cellular environment.[11,12]

The time delay between halothane exposure and measurement of mitochondrial function might also have reduced the magnitude of change in other components of the electron transport chain, and could have obscured other acute and reversible changes. It is also possible that permeabilisation of the muscle fibres, which is necessary for the SUIT protocol, might have limited the responses to halothane exposure. A further potential confounding factor in our study was that the halothane-exposed samples were maintained at approximate physiological length and tension, and were electrically stimulated during the halothane contracture test, whereas the baseline samples were not. While we think that the differences observed between our halothane-exposed and baseline samples are a result of the halothane exposure rather than other interventions, we were unable to demonstrate this because of a limited supply of human muscle tissue. We plan to address this in future studies using muscle tissue from *RYR1* knock-in mouse models.

In conclusion, we observed impaired mitochondrial function in permeabilised human MHS skeletal muscle which we hypothesise results from chronic elevation of cytoplasmic Ca^{2+} in MHS muscle that causes mitochondrial uncoupling and structural damage through increased ROS production. Exposure to halothane 2 vol% significantly increased OXPHOS and ETS capacity in MHS muscle, confirming a hypermetabolic response to halothane in MHS mitochondria with functional deficiency at baseline.

Authors' contributions

Conception and design of the study: PMH, MAS, JPB.
Conduct of experiments and data collection: LC, JPB.
Data analysis and interpretation: all authors.
Drafting of manuscript: LC, PMH.
Reviewed drafts of the manuscript and approved the final version: all authors.

Declaration of interests

PMH is an Editorial Board Member of the *British Journal of Anaesthesia*.

Funding

BJA/RCoA PhD studentship (MAS and PMH). National Institutes of Health (NIH) 2P01 AR-05235 (PDA, PMH).

Appendix A. Supplementary data

Supplementary data to this article can be found online at https://doi.org/10.1016/j.bja.2019.02.010.

References

1. Hopkins PM. Malignant hyperthermia – pharmacology of triggering. *Br J Anaesth* 2011; **107**: 48–56
2. Hopkins PM. Malignant hyperthermia: advances in clinical management and diagnosis. *Br J Anaesth* 2000; **85**: 118–28
3. Zorzato F, Fujii J, Otsu K, et al. Molecular cloning of cDNA encoding human and rabbit forms of the Ca2+ release channel (ryanodine receptor) of skeletal muscle sarcoplasmic reticulum. *J Biol Chem* 1990; **265**: 2244–56
4. Weiss RG, O'Connell KM, Flucher BE, Allen PD, Grabner M, Dirksen RT. Functional analysis of the R1086H malignant hyperthermia mutation in the DHPR reveals an unexpected influence of the III-IV loop on skeletal muscle EC coupling. *Am J Physiol Cell Physiol* 2004; **287**: C1094–102
5. Eltit JM, Bannister RA, Moua O, et al. Malignant hyperthermia susceptibility arising from altered resting coupling between the skeletal muscle L-type Ca2+

channel and the type 1 ryanodine receptor. *Proc Natl Acad Sci USA* 2012; **109**: 7923–8
6. Miller DM, Daly C, Aboelsaod EM, et al. Genetic epidemiology of malignant hyperthermia in the United Kingdom. *Br J Anaesth* 2018; **121**: 944–52
7. Hernández-Ochoa EO, Pratt SJP, Lovering RM, Schneider MF. Critical role of intracellular RyR1 calcium release channels in skeletal muscle function and disease. *Front Physiol* 2015; **6**: 420
8. MacLennan DH, Duff C, Zorzato F, et al. Ryanodine receptor gene is a candidate for predisposition to malignant hyperthermia. *Nature* 1990; **343**: 559–61
9. McCarthy TV, Healy JM, Heffron JJ, et al. Localization of the malignant hyperthermia susceptibility locus to human chromosome 19q12-13.2. *Nature* 1990; **343**: 562–4
10. Durham WJ, Aracena-Parks P, Long C, et al. RyR1 S-nitrosylation underlies environmental heat stroke and sudden death in Y522S RyR1 knockin mice. *Cell* 2008; **133**: 53–65
11. Giulivi C, Ross-Inta C, Omanska-Klusek A, et al. Basal bioenergetic abnormalities in skeletal muscle from ryanodine receptor malignant hyperthermia-susceptible R163C knock-in mice. *J Biol Chem* 2011; **286**: 99–113
12. Yuen B, Boncompagni S, Feng W, et al. Mice expressing T4826I-RYR1 are viable but exhibit sex- and genotype-dependent susceptibility to malignant hyperthermia and muscle damage. *FASEB J* 2012; **26**: 1311–22
13. Riazi S, Kraeva N, Hopkins PM. Malignant hyperthermia in the post-genomics era: new perspectives on an old concept. *Anesthesiology* 2018; **128**: 168–80
14. Britt BA, Endrenyi L, Cadman DL, Fan HM, Fung HY. Porcine malignant hyperthermia: effects of halothane on mitochondrial respiration and calcium accumulation. *Anesthesiology* 1975; **42**: 292–300
15. Gronert GA, Heffron JJ. Skeletal muscle mitochondria in porcine malignant hyperthermia: respiratory activity, calcium functions, and depression by halothane. *Anesth Analg* 1979; **58**: 76–81
16. Boncompagni S, Rossi AE, Micaroni M, et al. Mitochondria are linked to calcium stores in striated muscle by developmentally regulated tethering structures. *Mol Biol Cell* 2009; **20**: 1058–67
17. Isaacs H, Heffron JJ, Badenhorst M. Predictive tests for malignant hyperpyrexia. *Br J Anaesth* 1975; **47**: 1075–80
18. Lavorato M, Gupta PK, Hopkins PM, Franzini-Armstrong C. Skeletal muscle microalterations in patients carrying malignant hyperthermia-related mutations of the e-c coupling machinery. *Eur J Transl Myol* 2016; **26**: 6105
19. Cheah KS, Cheah AM, Fletcher JE, Rosenberg H. Skeletal muscle mitochondrial respiration of malignant hyperthermia-susceptible patients. Ca2+-induced uncoupling and free fatty acids. *Int J Biochem* 1989; **21**: 913–20
20. Thompson SJ, Riazi S, Kraeva N, et al. Skeletal muscle metabolic dysfunction in patients with malignant hyperthermia susceptibility. *Anesth Analg* 2017; **125**: 434–41
21. Hopkins PM, Rüffert H, Snoeck MM, et al. European Malignant Hyperthermia Group guidelines for investigation of malignant hyperthermia susceptibility. *Br J Anaesth* 2015; **115**: 531–9
22. Kuznetsov AV, Veksler V, Gellerich FN, Saks V, Margreiter R, Kunz WS. Analysis of mitochondrial function in situ in permeabilized muscle fibers, tissues and cells. *Nat Protoc* 2008; **3**: 965–76
23. Pesta D, Gnaiger E. High-resolution respirometry: OXPHOS protocols for human cells and permeabilized fibers from small biopsies of human muscle. *Methods Mol Biol* 2012; **810**: 25–58
24. Perry CG, Kane DA, Herbst EA, et al. Mitochondrial creatine kinase activity and phosphate shuttling are acutely regulated by exercise in human skeletal muscle. *J Physiol* 2012; **590**: 5475–86
25. Larsen S, Nielsen J, Hansen CN, et al. Biomarkers of mitochondrial content in skeletal muscle of healthy young human subjects. *J Physiol* 2012; **590**: 3349–60
26. Bezawork-Geleta A, Rohlena J, Dong L, Pacak K, Neuzil J. Mitochondrial complex II: at the crossroads. *Trends Biochem Sci* 2017; **42**: 312–25
27. Lemieux H, Blier PU, Gnaiger E. Remodeling pathway control of mitochondrial respiratory capacity by temperature in mouse heart: electron flow through the Q-junction in permeabilized fibers. *Sci Rep* 2017; **7**: 2840
28. López JR, Alamo L, Caputo C, Wikinski J, Ledezma D. Intracellular ionized calcium concentration in muscles from humans with malignant hyperthermia. *Muscle Nerve* 1985; **8**: 355–8
29. Lopez JR, Alamo LA, Jones DE, et al. [Ca2+]i in muscles of malignant hyperthermia susceptible pigs determined in vivo with Ca2+ selective microelectrodes. *Muscle Nerve* 1986; **9**: 85–6
30. Lopez JR, Kaura V, Diggle CP, Hopkins PM, Allen PD. Malignant hyperthermia, environmental heat stress and intracellular calcium dysregulation in a mouse model expressing the p.G2435R variant of the *RYR1* gene. *Br J Anaesth* 2018; **121**: 953–61
31. Guzy RD, Sharma B, Bell E, Chandel NS, Schumacker PT. Loss of the SdhB, but not the SdhA, subunit of complex II triggers reactive oxygen species-dependent hypoxia-inducible factor activation and tumorigenesis. *Mol Cell Biol* 2008; **28**: 718–31
32. Szabo I, Zoratti M. Mitochondrial channels: ion fluxes and more. *Physiol Rev* 2014; **94**: 519–608
33. Mailloux RJ, Harper ME. Mitochondrial proticity and ROS signaling: lessons from the uncoupling proteins. *Trends Endocrinol Metab* 2012; **23**: 451–8
34. Díaz-Vegas AR, Cordova A, Valladares D, et al. Mitochondrial calcium increase induced by RyR1 and IP3R channel activation after membrane depolarization regulates skeletal muscle metabolism. *Front Physiol* 2018; **9**: 791
35. McCormack JG, Denton RM. The effects of calcium ions and adenine nucleotides on the activity of pig heart 2-oxoglutarate dehydrogenase complex. *Biochem J* 1979; **180**: 533–44
36. Griffiths EJ, Rutter GA. Mitochondrial calcium as a key regulator of mitochondrial ATP production in mammalian cells. *Biochim Biophys Acta* 2009; **1787**: 1324–33
37. Figueroa L, Kraeva N, Manno C, Toro S, Ríos E, Riazi S. Abnormal calcium signalling and the caffeine–halothane contracture test. *Br J Anaesth* 2019; **122**: 32–41
38. Hanley PJ, Ray J, Brandt U, Daut J. Halothane, isoflurane and sevoflurane inhibit NADH:ubiquinone oxidoreductase (complex I) of cardiac mitochondria. *J Physiol* 2002; **544**: 687–93
39. Kayser EB, Morgan PG, Sedensky MM. Mitochondrial complex I function affects halothane sensitivity in *Caenorhabditis elegans*. *Anesthesiology* 2004; **101**: 365–72
40. Falk MJ, Kayser EB, Morgan PG, Sedensky MM. Mitochondrial complex I function modulates volatile anesthetic sensitivity in *C. elegans*. *Curr Biol* 2006; **16**: 1641–5

Handling editor: H.C. Hemmings